Chemical Geology 573 (2021) 120212

Contents lists available at ScienceDirect

Chemical Geology

journal homepage: www.elsevier.com/locate/chemgeo

Seasonal transformations of dissolved organic matter and organic phosphorus in a polymictic basin: Implications for redox-driven eutrophication

M.R. Kurek [a,b,*], M. Harir [c,e], J.T. Shukle [b], A.W. Schroth [d], P. Schmitt-Kopplin [c,e], G.K. Druschel [b]

[a] Department of Earth, Ocean and Atmospheric Science, Florida State University, Tallahassee, FL, USA
[b] Department of Earth Sciences, Indiana University-Purdue University Indianapolis, Indianapolis, IN, USA
[c] Helmholtz Zentrum München, German Research Center for Environmental Health, Research Unit Analytical BioGeoChemistry, Neuherberg, Germany
[d] Department of Geology, University of Vermont, Burlington, VT, USA
[e] Chair of Analytical Food Chemistry, Technical University of Munich, Freising-Weihenstephan, Germany

ARTICLE INFO

Keywords:
Freshwater DOM cycling
Freshwater organic P cycling
Eutrophication
Internal P loading

ABSTRACT

Redox-driven internal phosphorus (P) loading from lake sediments is a key process for propagating and sustaining cyanobacterial blooms in freshwater lakes. Missisquoi Bay in Lake Champlain, VT regularly experiences cyanobacterial blooms driven by internal P loading as well as from seasonal transitions, but the response of dissolved organic matter (DOM) to these changing conditions has previously not been investigated in this system and seldom in other redox-dynamic freshwaters. In this study, Fourier transform-ion cyclotron resonance mass spectrometry (FT-ICR MS) has been employed to explore the seasonal transformation and distribution of DOM, including organic P (DOP), from spring 2017 to winter 2018 along with high-frequency geochemical monitoring. DOM was largely composed of allochthonous compounds with unique molecules from seasonal autochthonous sources and greater proportions of N,S-containing formulae after the early summer bloom season and during the winter. DOM compositions from spring to late summer was more aliphatic during the early bloom season, while DOM between late summer to winter was more aromatic with greater similarities between the two seasons. In contrast, DOP compositions from all seasons were highly dissimilar and suggested a compartmentalized water column, where riverine DOP compounds that were degraded during transport and in surface waters were largely absent in the benthic DOP. Additional sediment core incubation experiments were implemented to study the effects of short-term oxygen limitation on DOM and DOP composition to better constrain potential redox-based drivers of their mobility between sediment and the water column. Short-term incubations suggested an increase in aliphatic DOM and new DOP compounds, with little change in aromatic DOM, suggesting selective mobilization driven by microbial iron(III) and manganese(IV) reduction. Together, these detailed FT-ICRMS data show, for the first time, how DOM and DOP from various sources respond to changing physical and geochemical conditions in redox-dynamic freshwaters, demonstrating how these compounds cycle in freshwater settings and likely impact nutrient bioavailability.

1. Introduction

Freshwater eutrophication is characterized by trophic shifts from excess nutrient concentrations, namely nitrogen (N) and phosphorus (P), resulting in polluted ecosystems and restriction of water resources (Smith et al., 1999). Aquatic primary producers consume excess nutrients promoting unrestricted phytoplankton growth and allowing for resilient cyanobacteria to outcompete algal communities, forming blooms of aggregated biomass (Mur et al., 1999). These blooms have resulted in adverse consequences for aquatic and human health including reduction of water clarity, fish kills, and production of unpleasant taste and odor compounds as well as harmful toxins (Paerl and Otten, 2013). Furthermore, blooms and their associated impacts are expected to increase globally due to temperature and hydrological effects promoted by climate change and anthropogenic pollution (O'neil et al., 2012; Nazari-Sharabian et al., 2018).

* Corresponding author at: Department of Earth, Ocean and Atmospheric Science, Florida State University, Tallahassee, FL, USA.
E-mail address: mrk19f@my.fsu.edu (M.R. Kurek).

https://doi.org/10.1016/j.chemgeo.2021.120212
Received 29 January 2021; Received in revised form 22 March 2021; Accepted 27 March 2021
Available online 30 March 2021

Anthropogenic nutrient pollution from point and nonpoint sources transports bioavailable P species, particularly inorganic orthophosphate (PO_4^{3-}), into freshwaters that can be utilized by cyanobacteria to promote and sustain bloom conditions (Paerl and Otten, 2013). Additionally, dissolved organic P (DOP) originates from both allochthonous (e.g., terrestrial) and autochthonous (e.g., aquatic) sources, serving as a potential pool of bioavailable P that can be mineralized through biological reactions and some abiotic processes (Baldwin et al., 2005; Bai et al., 2015; Klein et al., 2019). The dominant biological reactions governing DOP bioavailability are mediated by extracellular hydrolytic enzymes such as alkaline phosphatase and nucleotideases, or by direct microbial uptake of DOP (Heath, 2005). In both cases, DOP hydrolysis produces orthophosphate and dissolved organic matter (DOM), which diffuse into the water column, assimilate into biomass, or deposit with lake sediment. Freshwater DOM is a complex mixture of organic molecules with various functional groups, and like DOP, have both terrestrial and aquatic sources, each containing unique geochemical signatures (Koch et al., 2005; Kellerman et al., 2014; Kellerman et al., 2015; Johnston et al., 2019). DOM is also an integral part of aquatic energy transfer, representing a large portion of reactive carbon responsible for the global cycling of organic carbon to CO_2 (Tranvik et al., 2009; Drake et al., 2018) as well as sequestration of refractory compounds in the sediment (Valle et al., 2018). As aquatic DOM is supplied by primary producers and consumed by microorganisms to meet energy demands, DOP is also produced and metabolized to fulfill biological requirements. Therefore, in the context of eutrophication, the aquatic C and P cycles are linked through the exchange of phosphate groups between DOM and DOP.

Internal loading is a means by which P species, both inorganic and organic, are released from the sediment into the water column (Reynolds and Davies, 2001; Søndergaard et al., 2003; Ahlgren et al., 2011); often driving cyanobacterial blooms in shallow freshwaters (O'neil et al., 2012; Li et al., 2014). These blooms can produce anoxic conditions below the surface, resulting in nutrient release from the sediment (Rozan et al., 2002; Smith et al., 2011; Giles et al., 2016). This release is driven by the activity of anaerobic microbial communities that couple the metabolic oxidation of organic matter to the reduction of Mn(IV) first, followed by Fe(III) (Lovley, 1991). In these lakes, bioavailable Fe (III) originates from poorly-crystalline (oxy)hydroxide minerals with high adsorptive capacities for phosphate groups (Wang et al., 2013), and highly oxygenated DOM functional groups (Chassé and Ohno, 2016). Upon reductive dissolution of these minerals, P species and DOM are desorbed and mobilized from the sediment, fueling primary productivity in a positive feedback cycle where blooms are sustained from liberated nutrients and produce further anoxic conditions (Søndergaard et al., 2003; Parsons et al., 2017). The cycle breaks with bloom collapse from water column mixing or temperature decrease (Paerl and Otten, 2013), restoring dissolved oxygen as the terminal electron acceptor in the bottom water. This induces precipitation of Fe(III) (oxy)hydroxides and readsorption of P species and DOM (Reynolds and Davies, 2001; Smith et al., 2011; Voegelin et al., 2013), thereby recharging the sediment with nutrients.

Missisquoi Bay is a shallow, freshwater bay in Lake Champlain, hydrologically connected to both the Laurentian Great Lakes and the Atlantic Ocean, that experiences seasonal eutrophication driven partly by an internal loading process (Smith et al., 2011). Cyanobacterial blooms occur during the summer and become less frequent as the temperature decreases through fall (Isles et al., 2015). In winter the bay freezes over and creates a stratified water column with suboxic to hypoxic conditions in the bottom (Joung et al., 2017). Snowmelt in the spring loads P, Fe, and organic C into the bay from its watershed that supplies the initial excess nutrients for cyanobacterial blooms to develop when water temperatures are sufficiently warm (Isles et al., 2015; Isles et al., 2017b; Rosenberg and Schroth, 2017). The bay has been the target of several geochemical studies, including the use of long-term monitoring stations, resulting in abundant data regarding nutrient mobility and bioavailability (e.g., Smith et al., 2011; Giles et al., 2015; Schroth et al., 2015; Giles et al., 2016; Isles et al., 2017a, 2017b; Joung et al., 2017; Rosenberg and Schroth, 2017; Kurek et al., 2020); however, the contributions of DOM and DOP to internal loading have not been addressed in detail.

Fourier transform-ion cyclotron resonance mass spectrometry (FT-ICR MS) has been used extensively to investigate DOM molecular compositions in a multitude of freshwater lakes and rivers (e.g., Zhang et al., 2014; Wagner et al., 2015; Gonsior et al., 2016; Johnston et al., 2019) as well as incubated experiments (e.g., Dadi et al., 2017; Mostovaya et al., 2017; Valle et al., 2018). In this technique, DOM is routinely ionized in electrospray (ESI) with either negative mode (−), preferentially ionizing acidic and aromatic compounds, or positive mode (+), selecting for more basic and aliphatic compounds (Ohno et al., 2016). Neither approach has been widely applied to DOP analysis, in part due to the poor ionization efficiency of phosphate groups in ESI and low abundance of P in natural waters (Cooper et al., 2005); none to our knowledge have directly compared both. However, in eutrophic systems with elevated phosphorus concentrations, FT-ICR MS has demonstrated its utility for describing the distribution of organic P molecular classes in both freshwaters and leachates (Llewelyn et al., 2002; Brooker et al., 2018; Kurek et al., 2020). Though these approaches are largely qualitative due to the nature of FT-ICR MS data (Hertkorn et al., 2007), they provide insight into the mobility of DOP within aquatic systems and potential sources. Therefore, we employed a similar non-targeted FT-ICR MS approach in Missisquoi Bay combined with high frequency in situ sensor and electrochemical analyses to thoroughly describe the seasonal and intra-water column distribution of different DOM pools. The objectives of this study were: 1) to characterize the seasonal and spatial composition of DOM and DOP using FT-ICR MS in both ESI (−) and (+) and 2) to relate the observed DOM/DOP compositions with potential mobilizing events such as riverine input and benthic release to derive key processes driving DOM and DOP speciation.

2. Methods

2.1. Site description

Missisquoi Bay is a shallow, eutrophic basin of Lake Champlain that shares a border with Vermont (VT) and Quebec (see location map and details in Isles et al., 2015). The bay experiences harmful cyanobacterial blooms in the late summer months due to internal and external nutrient loading (Smith et al., 2011; Giles et al., 2016). The lake usually freezes completely during December with periodic thawing throughout the winter until April when it melts entirely. The watershed of the bay is mostly forested (70%) with agricultural (25%) and urban (5%) inputs spanning a total of 3100 km^2 (Joung et al., 2017). External nutrient loading is primarily supplied by surface runoff from three river systems: the Missisquoi, Pike, and Rock River. Major loading events occur in the spring following the melting of snowpack resulting in the highest sustained discharge and during the summer months when periodic storm events temporarily increase hydrologic surface flow paths to the bay (Rosenberg and Schroth, 2017).

2.2. Sampling and long-term monitoring

Water column samples from Missisquoi Bay were collected into acid-washed Nalgene bottles using a peristaltic pump during sampling events in May 2017, September 2017, and January 2018 along with manual YSI SONDE profiles (details in Schroth et al., 2015). On May 17, 2017 the total depth of the bay was recorded at 4.1 m and water samples were taken at the surface (top), 2.0 m (middle), and 3.2 m (bottom). On September 11, 2017 the total depth was 3.5 m with samples collected at the surface (top), 1.0 m, 2.0 m (middle), 3.0 m, and 3.1 m (bottom). Additionally, surface water from the Missisquoi River was sampled on September 13, 2017 at the USGS gaging station in Swanton, VT. On January 10, 2018 the total water column depth was 3.3 m and sampled

beneath ice cover at the surface (top), 2.0 m (middle), and 3.1 m (bottom). All water samples were immediately transported to the laboratory on ice, kept in the dark, and vacuum filtered through GF/F filters (precombusted at 450 °C for 5 h) for solid phase extraction. Sediment cores for incubation experiments were also collected on the same days as water sampling. The cores were obtained with a gravity coring device into acrylic tubes (6.7 cm diameter) and immediately transported to the laboratory on ice.

High-frequency water quality measurements were collected hourly in the Missisquoi Bay surface and bottom from June 28, 2017 to November 9, 2017 using an automated YSI vertical profiling system described in Giles et al. (2016). Surface and bottom water for total dissolved phosphorus (TDP) and soluble reactive phosphorus (SRP) were sampled weekly from July 28, 2017 to November 1, 2017 and analyzed optically using methods described in Joung et al. (2017). DOC concentrations in Missisquoi Bay vary minimally between seasons (mean = 5.1 mg L^{-1}, 4.2–6.1 90% CI) and have not varied significantly over the course of a 9-year study (Bowling et al., 2015).

2.3. Solid phase extractions

Solid phase extraction (SPE) procedures were adapted from Dittmar et al. (2008) to concentrate and desalt DOM for FT-ICR MS analysis. We determined that single PPL extractions from Missisquoi Bay were representative of the extractable DOM between replicates with low (<28% RSD) variability in molecular formulae and compositional homogeneity between extractions (Kurek et al., 2020). Immediately after filtering, DOM from water samples was extracted using 500 mg bond elut PPL columns, a styrene divinyl copolymer with the greatest and most consistent DOM recovery (Dittmar et al., 2008; Shakeri Yekta et al., 2012; Perminova et al., 2014; Swensen et al., 2014; Li et al., 2016). The columns were prepared by activating with 3 mL of methanol and washing with acidified water at pH 2. Then, filtered water samples (0.5–1.0 L) were acidified to pH 2 by dropwise addition of HCl and extracted through the columns by gravity feeding. After extraction, the columns were rinsed with acidified water at pH 2 and stored at −20 °C until analysis. Immediately before FT-ICR MS analysis, DOM from the columns was eluted with 5 mL of HPLC grade methanol into glass vials to a final concentration in the range of 0.34–0.66 mg C mL^{-1} based on mean DOC concentrations from Missisquoi Bay (Bowling et al., 2015).

2.4. Fourier transform ion cyclotron mass spectrometry

Methanolic extracts were analyzed using a Bruker Solarix 12 Tesla (Bruker Daltonics, Bremen, Germany) Fourier Transform-Ion Cyclotron Resonance Mass Spectrometer (FT-ICR MS) with electrospray ionization (ESI) in negative and positive mode. The extracts were prepared in methanol and then injected using a microliter pump at a flow rate of 120 μL h^{-1} with a nebulizer gas pressure of 138 kPa and a drying gas pressure of 103 kPa. A source heater temperature of 200 °C was kept, ensuring rapid desolvation of the ionized droplets. The spectra were zero filled to a processing size of 4 megawords and 500 scans were collected for each sample mass spectrum with the ion accumulation time tuned for each sample. Spectra in ESI (−) and ESI (+) contained on average around 17,000 peaks (See supplemental methods). All spectra were internally calibrated using an appropriate reference mass list to obtain a mass accuracy of less than 0.2 ppm. Data processing was conducted using Compass Data Analysis 4.1 (Bruker, Bremen, Germany) and formula assignments were processed by in-house software. The exact masses were defined and their molecular compositions were batch calculated by an in-house software tool (mass error 0.2 ppm). The formulae were validated by setting sensible chemical constraints (N-rule, oxygen-to-carbon (O/C) ratio ≤ 1, hydrogen-to-carbon (H/C) ratio $\leq 2n + 2(C_nH_{2n+2})$, element counts: C ≤ 80, H unlimited, O ≤ 60, $N \leq 5$, S ≤ 1, $P \leq 2$) with an automated theoretical isotope pattern comparison. Formula assignments were only considered if their mass peaks yielded a single theoretical formula with a corresponding ^{13}C peak (See supplemental methods). By incorporating these requirements, the amount of potential molecular formula was reduced, but the confidence in minimizing false assignments was maximized, especially for low abundance organic P molecules.

Final molecular formula assignments were branded into groups containing CHO(P), CHON(P), CHOS(P) and CHONS(P) molecular compositions, which were used to reconstruct the group-selective mass spectra. Chemical properties including the modified aromaticity index (AI), double bond equivalence (DBE), and carbon-normalized DBE (DBE/C) were calculated according to Koch and Dittmar (2006, 2016) as well as the average carbon oxidation state (CHO index) according to Mann et al. (2015). Molecular classes were also subjected to HPO_3-based Kendrick mass defect (KMD) analysis for identification of homologous series of compounds that differ in structure by just one HPO_3 mass group (Hughey et al., 2001). Post processing and statistical analysis of the filtered mass lists were conducted using Microsoft Excel and R (R Core Team, 2020) with the ggplot2 (Wickham, 2016), vegan (Oksanen et al., 2013), and eulerr (Larsson, 2018) packages.

2.5. Sediment core incubations

Cores collected in May and September were made anoxic by bubbling nitrogen gas into the surface water for one week (three days for the January core) in a cold-water bath (5 °C) and obscured from light using aluminum foil sheets. At the end of the incubations, 500 mL of the core water was siphoned into a glass beaker and filtered through a precombusted GF/F filter for solid phase extraction and FT-ICR MS. The degree of reduction for each core was determined by detecting dissolved Mn(II) and/or Fe(II) at or above the sediment-water interface (SWI) using in situ microelectrodes. Sediment cores from Missisquoi Bay have displayed spatially homogenous redox profiles (Smith et al., 2011), therefore only a single profile was completed for each core. Cyclic voltammetry was conducted using a three-electrode system on a model DLK-70 potentiostat (Analytical Instrument Systems, Inc.) with a gold amalgam microelectrode (working), an Ag/AgCl electrode (reference), and a platinum wire electrode (auxiliary) after established techniques (Brendel and Luther, 1995; Smith et al., 2011; Slowey and Marvin-DiPasquale, 2012). Further details are described in the supplementary information (Supplemental methods).

2.6. Analysis of model DOP compounds

A group of ^{31}P NMR-active compounds including, glucose-1-phosphate (G1P), adenosine-5′-monophosphate (AMP), and phenylphosphonic acid (PPA), were analyzed for their solid phase extraction and ionization efficiencies to determine if FT-ICR MS could yield previously detected organic P from Missisquoi Bay using ^{31}P NMR (Giles et al., 2015). G1P and AMP were selected to represent biomolecules with phosphomonoester bonds (O—P) while PPA was chosen to represent compounds with phosphonate bonds (C—P) with higher molecular weights that could easily be ionized in FT-ICR MS. Stock solutions were made by dissolving each compound in Milli-Q water to final concentrations of 88 mg L^{-1} G1P, 68 mg L^{-1} AMP, and 103 mg L^{-1} PPA. The solutions were extracted using the PPL SPE procedure and the permeate (the liquid that passes through the column during extraction) was collected for total P quantification. The permeates were diluted 1:10 in Milli-Q water and analyzed on a Perkin Elmer ICP-OES for total P. Sample reproducibility, calculated from three replicates, was within 5%. The samples were blank-corrected, and percent retention was calculated as the stock concentration minus the eluted concentration relative to the stock concentration for each compound. The PPL columns were then stored at −20 °C prior to elution for FT-ICR MS (section 2.4).

2.7. Statistical analysis

Non-metric multidimensional scaling (NMDS) was implemented to construct a "seasonal map" of Missisquoi Bay DOM due to the minimal assumptions it makes regarding the distribution and linearity of the input data (Paliy & Shankar, 2016). NMDS biplots (k = 2, stress <0.1) were made using the vegan package in R (Oksanen et al., 2013) from Bray-Curtis distances using mean square root transformed parameters derived from the FT-ICR MS spectra (e.g., H/C, O/C, N/C, etc.) in each ionization mode and data from the SONDE profiles. All reported variables were statistically significant ($\alpha = 0.05$).

Linear correlations between the FT-ICR MS variables and a subset of the SONDE variables were also modeled in R with the Hmisc package (Harrell Jr., 2020) and their correlation coefficients reported at the $\alpha = 0.05$ significance level. Additionally, mean values of the FT-ICR MS variables between the bottom water and incubated core water were compared using a two-sample *t*-test in R.

3. Results

3.1. Seasonal water column sensor and geochemistry data

Automated SONDE profiles measured temperature (T), dissolved O_2 (DO), pH, chlorophyll-a (Chl a), and phycocyanin (blue-green algae pigment, [BGA]) at the surface (black line) and bottom (red line) (Fig. 1A-E). Throughout the summer and late fall, pH, DO, Chl a, and phycocyanin increased during warmer surface temperatures and were higher in the surface than the bottom in two distinct periods. The first period occurred from early July to early September while the second period was from mid-September to early October, consistent with past data from Missisquoi Bay (Giles et al., 2016). Total dissolved P (TDP) in the surface and bottom (solid lines) decreased from mid-July to November while soluble reactive P (SRP) (dashed lines) gradually increased (Fig. 1F).

Individual SONDE profiles measured the same day as water sampling for May, September, and January are provided in the supplemental information (Fig. S.1). In general, Chl a, phycocyanin, and pH decreased from May to January while temperature followed the order of September > May > January. DO was uniform through depth in May (109% sat.) and September (95% sat.), but more stratified in January (changing from 97 to 55% sat. with depth).

3.2. Model DOP compound retention and ionization

Retention of the model DOP compounds in the PPL columns was variable following the order of PPA (41.7%) > G1P (30.5%) > AMP (3.5%). In ESI (−), both G1P and PPA were identified in their mass spectra, but AMP was not. Furthermore, possible AMP degradation products such as adenosine, glucose, G1P, or adenine were also absent from the mass spectrum. In ESI (+), none of the model compounds were detected, though the presence of adenosine in the AMP spectra suggested the potential degradation product was preferentially ionized over AMP. The presence of all the organic P standards in the PPL columns indicates that SPE can retain some of the same compounds that are ^{31}P NMR-active, but their variability in the FT-ICR MS spectra suggests that their detection is highly dependent on ionization mode. By considering DOP compounds in both ESI (−) and ESI (+) spectra, we extended our analytical window to reveal functionally different molecules whose compositions are consistent across replicate PPL extractions (Kurek et al., 2020).

3.3. FT-ICR MS analysis of water column DOM

Analysis of assigned molecular formulae was separated into non-P-containing (DOM) and P-containing (DOP) molecules to identify trends within the two groups. Compounds were further grouped into molecular classes based on their atomic composition and visualized using van Krevelen diagrams which display the formulaic H/C ratio against the formulaic O/C ratio of each molecule. Points in van Krevelen space represent molecular formulae which may consist of many isomers following predictable trends (Hertkorn et al., 2007). In general, compounds with higher H/C are more saturated and aliphatic, while those with lower H/C are unsaturated. Similarly, molecules with higher O/C values are more oxygenated than those with lower O/C. Commonality between samples was assessed by the relative molecular formulae shared between FT-ICR MS spectra, visualized in size-proportional Venn diagrams. Samples that share many of the same formulae have a high commonality corresponding to a greater area of intersection, whereas those that share few formulae have a low commonality and are more "unique".

A matrix of the DOM and DOP compounds in ESI (−) and ESI (+) is depicted in Figs. 2 and 3, supplemented with mass spectral characteristics in table S.1. Samples in each column were collected from the same season while samples across each row are from the same depth. Likewise, Venn diagrams at the top of each column describe the presence/absence of each molecule between the water column spectra and the

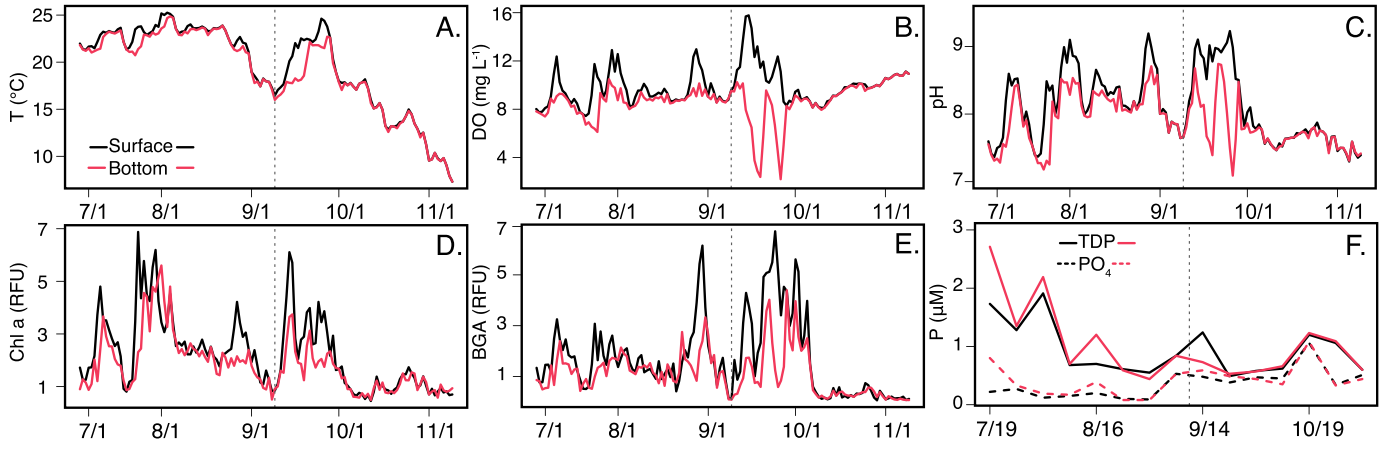

Fig. 1. High-frequency YSI SONDE data collected in from June 28, 2017 to November 9, 2017 for (A) temperature, (B) dissolved oxygen, (C) pH, (D) chlorophyll-a (Chl a), and (E) blue-green algae phycocyanin (BGA) in the surface (black) and bottom water (red). (F) Phosphorus was measured from July 28, 2017 to November 1, 2017 as total dissolved (solid lines) and soluble reactive (dashed lines) in the surface (black) and bottom water (red). The vertical dashed line indicates the water column sampling on September 11, 2017. (For interpretation of the references to colour in this figure legend, the reader is referred to the web version of this article.)

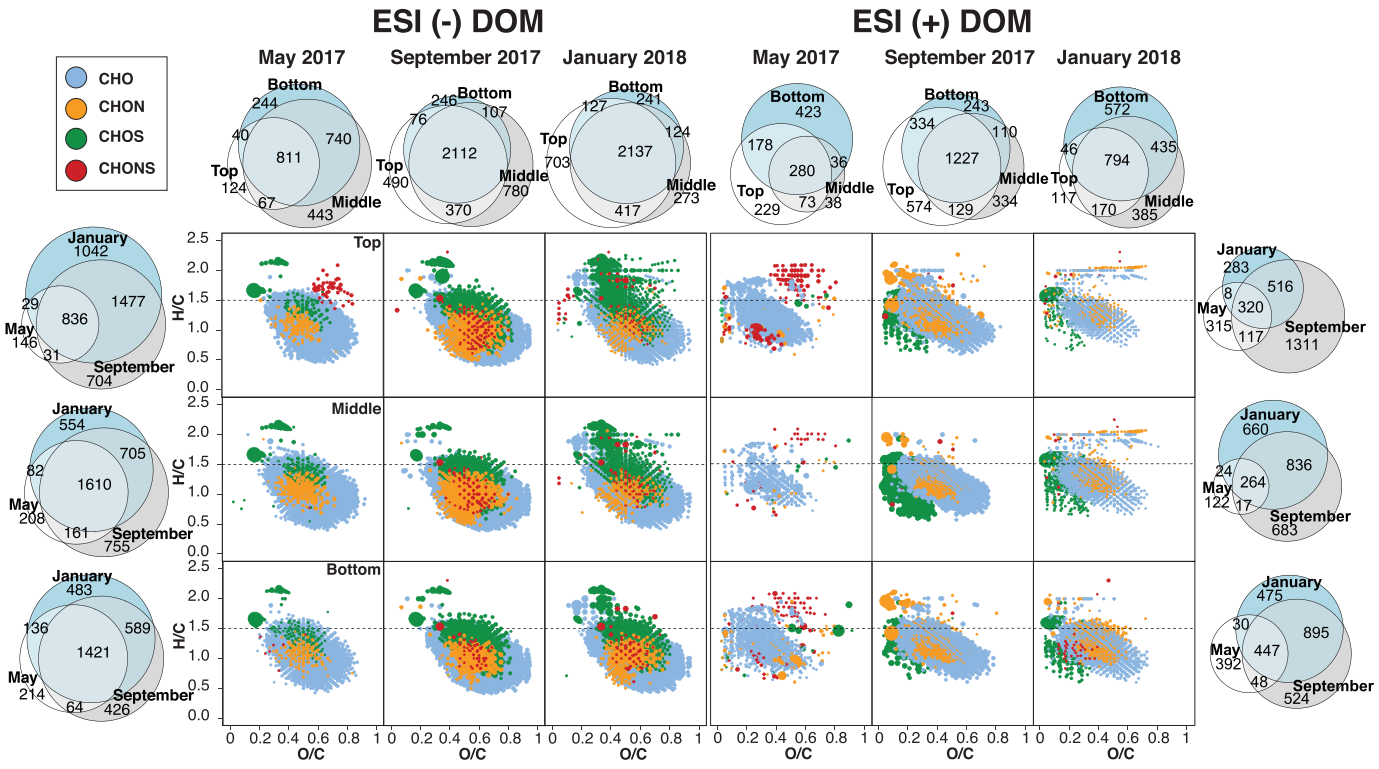

Fig. 2. van Krevelen diagrams of assigned non-P-containing formulae ionized in ESI (±) FT-ICR from the Missisquoi Bay water column. A grey dashed line at H/C = 1.5 represents the molecular lability boundary (MLB). Venn diagram sizes are proportional to the total number of formulae and correspond to samples in the water column of the same month (columns) and depths across different months (rows). Elemental compositions bearing combinations of C, H, O, N and S atoms are defined as follows: blue (CHO), green (CHOS), orange (CHON) and red (CHONS). Bubble sizes are scaled proportionally to m/z ion intensity.

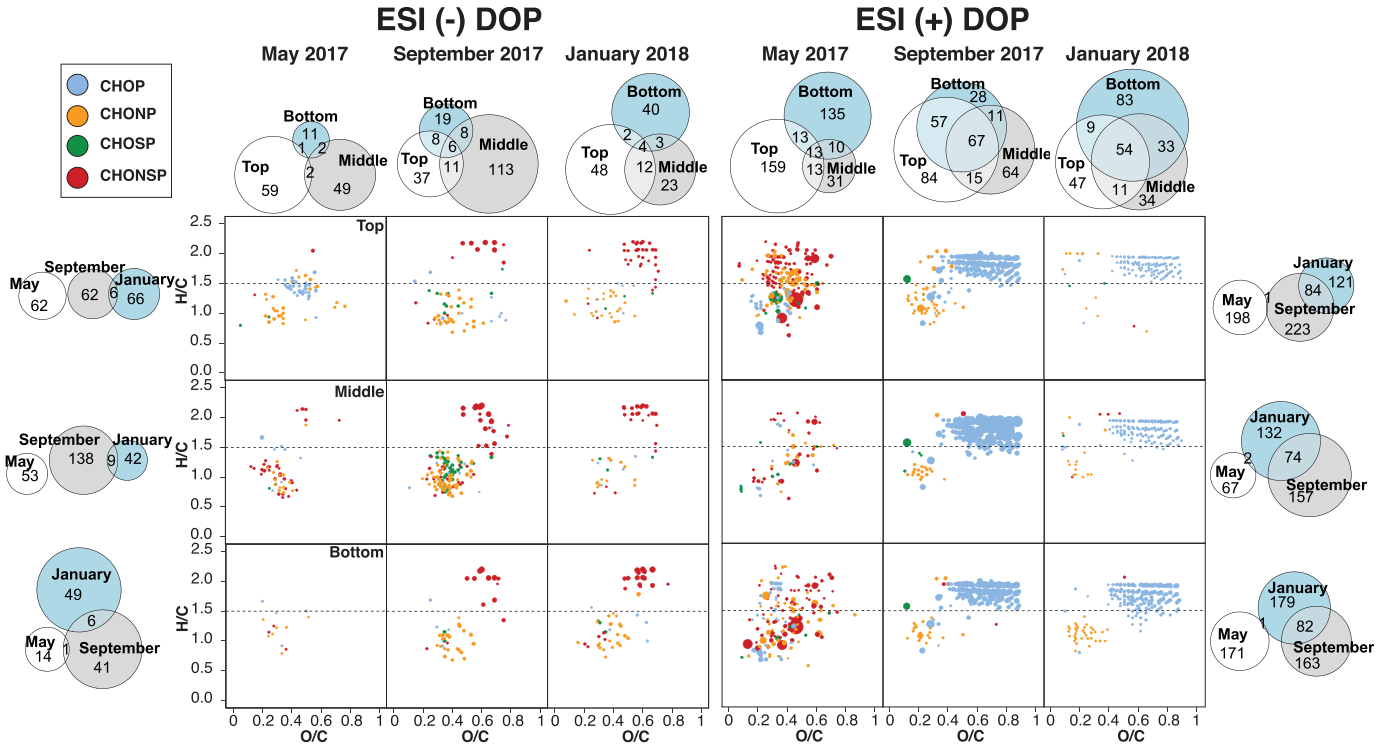

Fig. 3. van Krevelen diagrams of assigned P-containing formulae ionized in ESI (±) FT-ICR MS from the Missisquoi Bay water column. A grey dashed line at H/C = 1.5 represents the molecular lability boundary (MLB). Venn diagram sizes are proportional to the total number of formulae and correspond to samples in the water column of the same month (columns) and depths across different months (rows). Colour-code represent the elemental compositions bearing blue (CHOP), orange (CHONP), green (CHOSP), and red (CHONSP) molecular compositions. Bubble sizes are scaled proportionally to m/z ion intensity.

Venn diagrams at the end of each row correspond to the same depth across each season. A molecular lability boundary (MLB) at H/C = 1.5, classifies compounds that are generally more biolabile (D'Andrilli et al., 2015) and is depicted as a grey dashed line in the van Krevelen diagrams. Formulae that plot above this line are thought to share characteristics similar to biolabile compounds (D'Andrilli et al., 2015).

3.3.1. FT-ICR MS DOM

In ESI (−), the May water column DOM had the lowest molecular diversity, defined as the total number of assigned formulae (Fig. 2, vertical Venn diagrams; Table S.1), and the lowest commonality within the water column compared to September and January. May was mostly composed of CHO-containing formulae with a unique cluster of CHONS formulae in the surface above the MLB, while September and January had more CHON and CHOS formulae than in May (Fig. 2, Fig. S.2). From September to January, there was an overall increase in saturated compounds (Table S.1) and more CHOS formulae above the MLB (Fig. 2). Across all seasons, formulae from the same depth were less common through time except between September and January which shared more formulae with each other than with May (Fig. 2, horizontal Venn diagrams).

Water column DOM ionized in ESI (+) was more saturated, less oxygenated, and had lower molecular diversity than in ESI (−) (Table S.1). Molecular class distributions also differed with more saturated CHON formulae above the MLB and CHOS formulae at lower H/C and O/C ratios (Fig. 2). Proportionally, DOM analyzed in ESI (+) ionized more unique compounds in each sample than in ESI (−). Similar to ESI (−), May differed from September and January, having the lowest molecular diversity and commonality within the water column as well as being almost entirely composed of CHO formulae with the exception of CHONS clusters above the MLB (Fig. 2, Fig. S.2). September and January both increased in CHON and CHOS-containing formulae with similar proportions (Fig. S.2), but September had greater commonality within the water column (Fig. 2). At each depth, the proportion of formulae shared across the seasons were lower than in ESI (−), with January and September still sharing more formulae with each other than with May (Fig. 2).

3.3.2. FT-ICR MS DOP

Unlike the DOM trends, DOP compositions in ESI (−) were less uniform within the water column, with most molecules unique to each depth (Fig. 3, vertical Venn diagrams). Most DOP compounds were CHONP or CHONSP-containing with formulae above the MLB increasing from May to January (Fig. 3). DOP compounds were also largely unique to each season, with only a few formulae shared between September and January (Fig. 3). In contrast, the ESI (+) spectra contained proportionally more DOP compounds than in ESI (−), comprising 6.9 to 20.7% of all formula assignments (Fig. S.2). DOP compounds were also largely unique to each depth especially in May, but overall had more intra-water column commonality than in ESI (−) (Fig. 3). The ESI (+) May water column consisted of mainly CHONP, and CHONSP-containing formulae (Fig. 3). However, in September and January there was a shift to mostly CHOP-containing formulae. These formulae plotted above the MLB spanning an O/C range of 0.4–0.9 while the other formulae were more unsaturated, clustering in a lower and narrower O/C range (Fig. 3). May was clearly distinct from September and January, sharing almost no formulae with either month, while September and January had proportionally more commonality with each other than in ESI (−) (Fig. 3, horizontal Venn diagrams).

3.4. Linking environmental variables to DOM composition

FT-ICR MS data are information-dense. They contain detailed descriptions of molecules from each sample but make larger scale relationships between multiple samples difficult to conceptualize. Combining water column FT-ICR MS data and water quality SONDE data through ordination provided a holistic view of how DOM was processed and mobilized (Fig. 4). NMDS biplots revealed that differences in bulk molecular properties (e.g., O/C, H/C, AI etc.) guided the overall DOM variations from May to January that were seen in van Krevelen space (Fig. 2, Fig. 3). DOM from ESI (−) (Fig. 4A) and ESI (+) (Fig. 4B) were clearly separated along NMDS1 by season and strongly guided by phycocyanin, chlorophyll-a, and pH as well as aliphaticity (H/C) and S-content (CHOS and S/C). NMDS2 separated samples by depth and were strongly guided by temperature and FT-ICR MS variables characteristic of each ionization mode such as N- and P-content as well as aromaticity (AI) and oxygenation (O/C, CHO index) in ESI (+) (Fig. 4B).

Relationships between temperature, DO, pH and the FT-ICR MS DOM were further investigated through analysis of significant ($\alpha = 0.05$) correlations (Fig. 5). Differences in ionization revealed negative correlations between temperature and pH with S/C in ESI (−) (Fig. 5A) and positive correlations with N/C in ESI (+) (Fig. 5C). Subsequently, the analysis was focused on formulae that were common in both ionization modes to target the formulae that one may encounter in either ionization mode (Fig. 5A). We recognize that by restricting our analysis to the peaks common between both modes we are selecting for compounds with the most ionizable functional groups. However, by doing this we are consistently comparing the same fraction of DOM compounds spatially and temporally and minimizing the effect of lower intensity peaks that are unique to either ESI (−) or ESI (+). In the common fraction, temperature correlated negatively with H/C and positively with the CHO index and AI, while pH only correlated positively with AI. In contrast, DO correlated positively with H/C and negatively with AI (Fig. 5A). Correlations between AI and H/C with DO also appeared separately in the ESI (−) and ESI (+) spectra (Fig. 5B, C), suggesting this trend occurred across various functional groups.

3.5. Fluvial DOM

DOM from the Missisquoi River was compared with surface water from September to investigate the contribution of allochthonous DOM and DOP to the water column. Riverine DOM was mostly composed of CHO and CHON-containing formulae in both ESI (−) (Fig. S.4A) and ESI (+) (Fig. S·4B) that had similar H/C and O/C ranges as the surface water. The riverine ESI (+) DOM also contained more DOP compounds than the ESI (−) DOM (Fig. S.4) and was composed of the same cluster of aliphatic formulae above the MLB that were found in the ESI (+) water column. In contrast, riverine DOP in ESI (−) was more dispersed with lower intensities, similar to the water column DOP (Fig. 3).

DOM formulae present in both ionization modes from surface water were highly similar to DOM from the Missisquoi River (Fig. 6A). 82.7% of the riverine DOM formulae were present in the surface water in ESI (−) (red lines) decreasing through the water column to 62.9% at the bottom with a similar trend for ESI (+) (blue lines), and the shared formulae (purple lines) (Fig. 6A). Riverine loss also occurred in the DOP compounds, but at a greater percentage compared to DOM (Fig. 6). In ESI (−), the surface only contained 23.8% of riverine DOP and decreased to 1.6% at the bottom. Commonality was greater in ESI (+) with the surface containing 67.7% of riverine DOP formulae and decreasing to 27.3% at the bottom (Fig. 6B).

3.6. DOM transformations during incubation

Missisquoi Bay sediment cores were studied to observe the mobilization of DOM and DOP from sediment during periods of short-term oxygen limitation (e.g., bloom onset conditions). Reducing conditions at the SWI were achieved up to seven days after incubation and were confirmed by the presence of Mn(II) and/or Fe(II) and absence of O_2 at or above the SWI (Fig. 7). DOM from the reduced cores was analyzed using FT-ICR MS and compared to the bottom water for each month to investigate changes in chemical composition. Only the formulae common between ESI (−) and ESI (+) in each sample were considered for

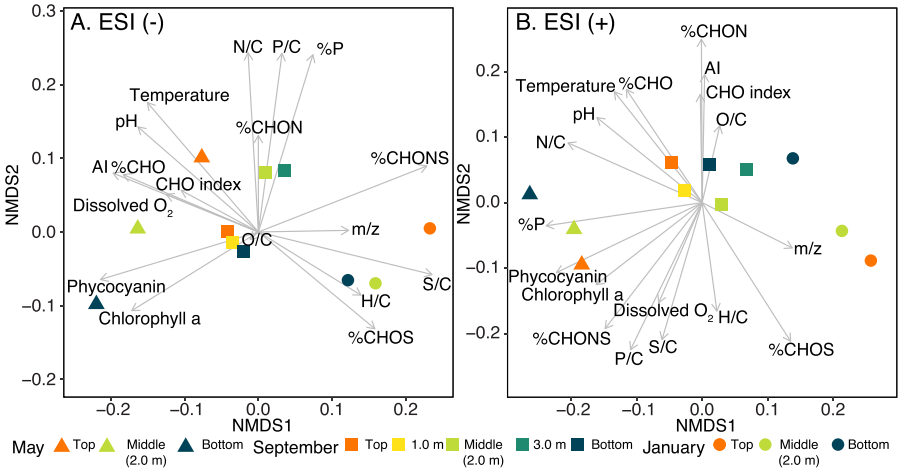

Fig. 4. NMDS biplots (k = 2, stress <0.1) of water column samples from this study using data obtained from manual SONDE profiles and individual mass spectra in (A) ESI (−) and (B) ESI (+). Distances are calculated using Bray-Curtis dissimilarity matrices of samples from May 2017 (triangles), September 2017 (squares), and January 2018 (circles). Variables are represented by grey arrows with their relative lengths corresponding to their influence on each sample.

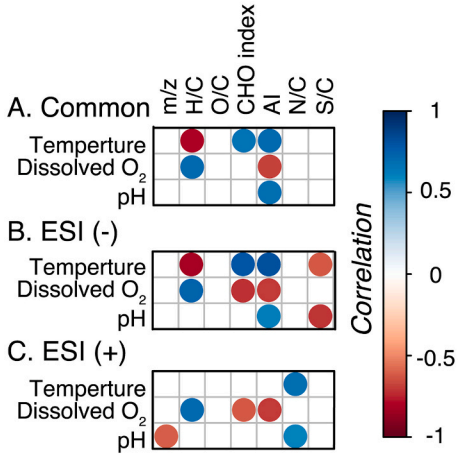

Fig. 5. Correlation table of temperature (°C), dissolved oxygen (mg L^{-1}), and pH from manual SONDE profiles of Missisquoi Bay with mean m/z (Da), H/C, O/C, CHO index, AI, N/C, and S/C obtained from FT-ICR MS formulae (A) common in both ionizations, (B) in ESI (−), and (C) ESI (+). Circles represent statistically significant (α = 0.05) correlations and are colored by Pearson's correlation coefficient (positive = blue, negative = red). (For interpretation of the references to colour in this figure legend, the reader is referred to the web version of this article.)

this analysis (see section *3.4*). Despite the seasonal heterogeneity of the sediment, compounds in all seasons shifted to significantly (α = 0.05) lower mean masses, AI, and CHO indices while increasing in H/C (Table 1) compared to the bottom water after each incubation. O/C values were also lower in the cores, though not significantly in May (Table 1).

Unlike DOM, changes in DOP formulae between the bottom water and incubation were minimal with a consistent percentage of P-containing formulae and P/C ratios (Table S.2). Few DOP molecules from the bottom water were retained after the incubation, especially in ESI (−), but an entirely different set of DOP compounds were ionized (Table S.2). Due to the minimal commonality of DOP between ESI (−) and ESI (+), DOP compounds from both ionization modes were grouped together and compared between the bottom water and incubations. Overall, reduction resulted in DOP compounds with significantly (α = 0.05) lower masses, CHO indices, and higher H/C with no significant trends in O/C or aromaticity (Table S.3).

4. Discussion

4.1. Seasonality of Missisquoi Bay DOM composition

In Missisquoi Bay, May represented the "pre-bloom" season at the end of the spring melt (Fig. S.5) and the beginning of summer with rising temperatures, pH, and increased phototrophic activity (Isles et al., 2017a; Fig. S.1). May DOM was mostly composed of unsaturated CHO formulae (Fig. 2) likely loaded into the bay from the recent spring melt (Fig. S.5), but also contained distinct aliphatic CHONS formulae that are likely characteristic of diverse algal metabolites (Zhang et al., 2014; Ly et al., 2017), coincident with the onset of autochthonous production from spring phytoplankton blooms (Isles et al., 2017a; Fig. 1). As surface temperatures increased through the summer (Fig. 1A), productivity from algae and cyanobacteria increased, forming an early season bloom in July before collapsing in early September during a brief cool period (Fig. 1D,E).

During the September sampling, more oxidized DOM had accumulated in the bay (Fig. 5) with greater homogeneity between each depth (Fig. 2) following bloom collapse, suggestive of vertical mixing (Fig. S.1). Much of the DOM from May was still present in the September water column but the overall DOM composition had experienced biological processing resulting in the production of many unique formulae (Fig. 2; Fig. S.2), possibly from various bacteria and microalgae (Bittar et al., 2015b; Mangal et al., 2016; Kamjunke et al., 2017a). Thus, the September DOM increased in chemodiversity (Table S.1), heteroatom (N,S) content, and aliphatic compounds (Fig. 2; Fig. S.2), illustrating a relatively short diversification event of aquatic DOM between early to late summer. Additionally, photooxidation may have been important for production of saturated DOM during stratified summer periods (Gonsior et al., 2013), but these highly oxygenated photoproducts were absent from the September surface DOM following the bloom period (Fig. 2; Table S.1), suggesting that vertical mixing could also be responsible for redistributing DOM through shallow water columns.

The September DOM was also compared to the Missisquoi River DOM to investigate the distribution of terrestrial inputs (Fig. 6). Missisquoi River DOM was composed of mainly high O/C and low H/C formulae (Fig. S.4) likely representing allochthonous compounds sourced from the watershed (Kellerman et al., 2015; Wagner et al., 2015; Gonsior et al., 2016). Between both ionization modes (Fig. 6A, red and blue lines) and formulae common between the two (Fig. 6A, purple line), most of the original riverine DOM was retained in the surface water with over 60% still present in the bottom water. This distribution suggests that a large fraction of allochthonous DOM arriving into the bay was

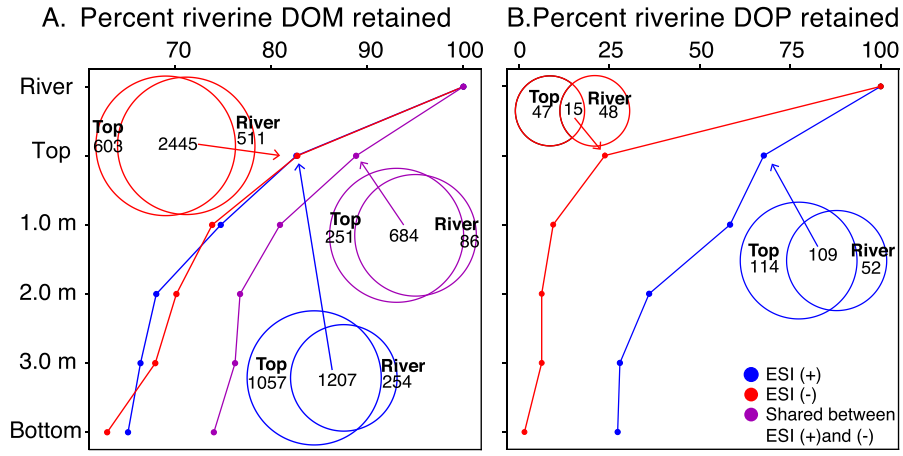

Fig. 6. Line plots depicting the percentage of formulae from the Missisquoi River detected in the September water column at each depth for (A) DOM and (B) DOP (P-containing formulae). Colors correspond to formulae in ESI (−) (red), ESI (+) (blue), and common between both ionization modes (purple). Proportional Venn diagrams of formulae shared between the riverine and surface water DOM are colored according to the same colour scheme as the connecting lines. (For interpretation of the references to colour in this figure legend, the reader is referred to the web version of this article.)

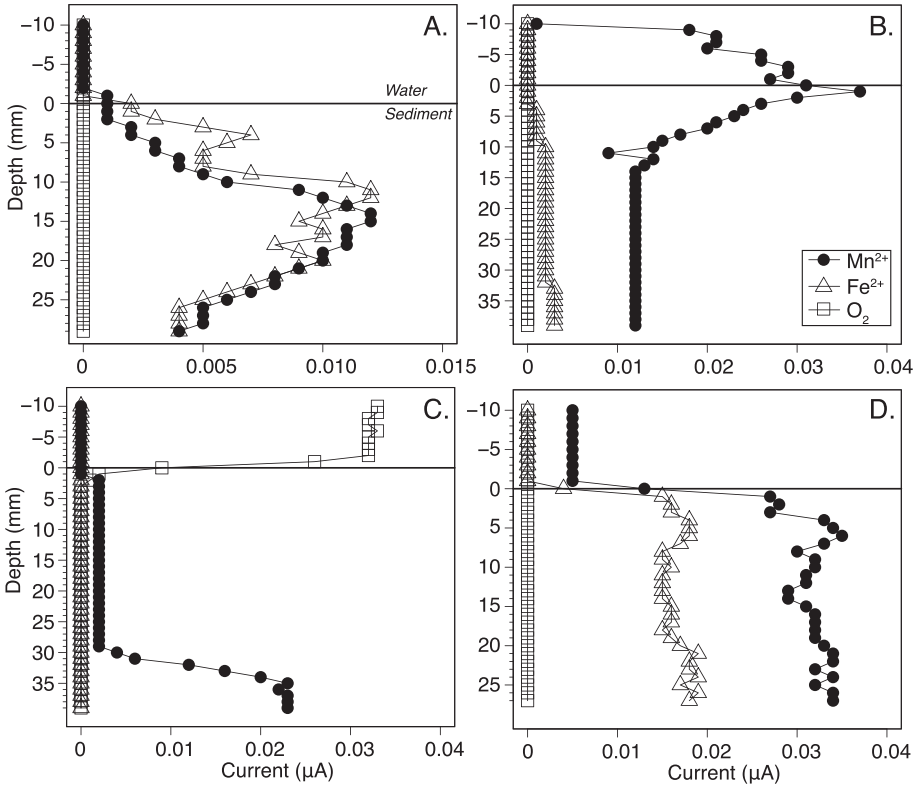

Fig. 7. Depth profiles of electroactive chemical species from incubated Missisquoi Bay sediment cores. Measured current intensities of Mn^{2+} (solid circles), Fe^{2+} (open triangles), and O_2 (open squares) are proportional to chemical concentrations. Chemical species are electroactive on the Hg-amalgam at a specific potential referenced to an Ag/AgCl electrode; for details see Brendel and Luther (1995). The sediment-water interface (SWI) is depicted by a solid black line at depth = 0 mm. Profiles correspond to (A) reducing, May 2017; (B) reducing, September 2017; (C) oxic, September 2017; (D) reducing, January 2018.

Table 1
Calculated mean values of H/C, O/C, m/z, CHO index, and AI before and after (before | after) reduction for ions common between both ionization modes where the first value indicates bottom water and the following value indicates reduced core water. All differences between bottom water and reduced core water are statistically significant (α = 0.05), except for May O/C indicated by an asterisk (*).

	H/C	O/C	m/z (Da)	CHO index	AI
May	1.16 | 1.23	0.42 | 0.41*	408.7124 | 394.7072	−0.33 | −0.41	0.33 | 0.29
September	1.17 | 1.25	0.45 | 0.43	440.2091 | 415.1408	−0.26 | −0.38	0.31 | 0.27
January	1.17 | 1.25	0.43 | 0.41	440.8340 | 423.4111	−0.31 | −0.44	0.32 | 0.27

incorporated into the water column and resistant to degradation. In contrast, DOM fractions unique to the surface water (Fig. 6A Venn diagrams) represented only a minority of compounds in ESI (−) (Fig. 6A red Venn) and the shared formulae (Fig. 6A purple Venn), but was almost half of the compounds in ESI (+) (Fig. 6A blue Venn). The unique fractions likely represent a combination of autochthony and degradation byproducts (Koch et al., 2005; Bittar et al., 2015a, 2015b) that were more abundant in ESI (+) due to the ionization preference of alcohols and amines (Sleighter and Hatcher, 2007), which are often associated with autochthonous DOM (Zhang et al., 2014).

Following a brief cool period in September, surface temperatures increased (Fig. 1A) and discharge into the bay stagnated (Fig. S.5), which supported favorable conditions for a late season algal and cyanobacterial bloom (Fig. 1D, E) promoting water column redox gradients (Fig. 1B). Although we did not sample DOM from this period, we suspect

DOM compositions would have been similar to the stable allochthonous compounds seen in September (Fig. 6A), with more saturated and N- and S-containing formulae at the surface from heightened productivity (Fig. 1D, E). However, these compositions would only be transient as high discharge periods in November following the bloom collapse (Fig. S.5) would have decreased water residence time and flushed out or diluted much of the processed DOM (Kellerman et al., 2014) replacing these bloom compounds with allochthonous DOM.

By January 2018, discharge had subsided to baseflow (Fig. S.5) and the surface had frozen over (Fig. S.1; Joung et al., 2017), cutting off the water column from terrestrial and atmospheric influence. The water column reflected this change in weather, with greater geochemical stratification (Fig. S.1) and DOM composition differing from the early and late summer periods in ESI (−) and ESI (+) (Fig. 4). Overall, January DOM was closer in composition and shared more common formulae with September than with May (Fig. 2, Fig. 4), which could have been partly due to winter ice cover attenuating the photodegradation of aromatic compounds (Stubbins et al., 2010; D'Andrilli et al., 2013; Gonsior et al., 2013). However, January differed by its unique aliphatic content, consisting of more formulae above the MLB and S-containing formulae (Fig. 2, Fig. 4). Furthermore, the increase in high-intensity aliphatic CHOS-containing series (Fig. 2) was probably biogenic since reactive sulfur species (e.g., HS-, polysulfides) have never been detected in this water column making abiotic sulfurization improbable. The increases in aliphatic molecules underneath the ice could be explained by a combination of lessened riverine input during winter and a shift in microbial activity to heterotrophy resulting in distinct autochthonous DOM (Romano et al., 2014; Morling et al., 2017; Johnston et al., 2019). Since microorganisms both produce and consume labile organic matter (Guillemette and del Giorgio, 2012), the unique January compounds are likely a combination of both processes. The resulting autochthonous DOM is consumed preferentially over allochthonous DOM (Kamjunke et al., 2017b; Mostovaya et al., 2017) and could serve as a source of labile organic carbon following the thaw period when mixing is facilitated by atmospheric oxygen in the water column and increased surface temperatures (Schroth et al., 2015; Joung et al., 2017).

4.2. Missisquoi Bay DOP cycling

FT-ICR MS analyses (using SPE and ionization in both modes) complemented with quantitative analysis of TDP and SRP concentrations revealed spatial and temporal DOP dynamics that has not been previously investigated as a component of bloom activity in eutrophic freshwater lakes. A depletion of DOP through the early summer bloom period was evident from the decrease of TDP from July to September as the SRP concentration remained relatively constant (Fig. 1F). This decrease in both the surface and bottom water suggested that DOP was being consumed, possibly as a source of phosphorus given that SRP concentrations were low during this period and productivity was high (Fig. 1B, D–F). The decrease of this DOP fraction was also accompanied by a shift in molecular DOP compositions between May and September (Fig. 3) likely due to the microbial processing of organic matter during the early summer bloom period (Bittar et al., 2015a, 2015b; Fig. 2). Additionally, the fraction of SRP relative to TDP in the surface differed from the bottom in Missisquoi Bay, particularly in early July and late Summer (Fig. 1F), suggesting that there are spatial differences in DOP cycling even within meters of shallow freshwater. DOP formulae also displayed poor intra-water column commonality during each timepoint and between seasons in both ionization modes (Fig. 3), further suggesting that DOP in Missisquoi Bay was rapidly altered. Though we recognize that the absence of shared DOP compounds between samples may be due to additional factors, including ion suppression of DOP compounds by more highly ionizable functional groups (Sleighter and Hatcher, 2007), the changes seen in the FT-ICR MS DOP compounds agree with the quantitative changes between organic and inorganic P species (Fig. 1F).

Kendrick mass defect analysis of HPO_3 unit loss/addition pairs also revealed that many of the DOP compounds were possibly linked to precursor DOM molecules within the water column by the addition/removal of a single phosphate group (Fig. S.3). Although the structure of these DOP molecules remains uncharacterized, the vast majority of aquatic DOP compounds contain either phosphate or phosphonate functional groups (Baldwin, 2013) differing from DOM by HPO_3 units. The presence of these Kendrick series suggests that many of the DOP compounds could be hydrolyzed (HPO_3 loss), producing DOM and inorganic phosphate groups, which could be scavenged by microorganisms (Heath, 2005; Baldwin, 2013). The Kendrick series also supported the differences in DOP compositions seen between each season as evidenced by their low commonality and stoichiometric differences, particularly through the early summer (Fig. 3) where DOP concentrations were high (Fig. 1F). Between September and January, DOP stoichiometries were more similar in both ionization modes with greater shared formulae than with May, suggesting less consumption of DOP as SRP became more available during and after the late season bloom (Fig. 1F) and when primary productivity was low (Fig. S.1).

During the low-productivity period in September, DOP compounds in Missisquoi Bay were highly dissimilar from riverine DOP both at the surface and through the water column (Fig. 6B), in contrast to the DOM (Fig. 6A). This dissimilarity suggests that DOP compounds were actively supplied to the mouth of the bay from allochthonous sources, but absent in the water column after traveling through the Missisquoi River delta. Such lateral transport has also been shown to degrade DOP in other wetlands, resulting in the retention of only a minimal number of allochthonous compounds and could be a source of SRP to the surface water through hydrolysis (Llewelyn et al., 2002; El-Rifai et al., 2008). Although these comparisons were only drawn in September, it is likely that transport and degradation processes were different in winter and spring. DOP external loading in winter was lower due to ice cover restricting riverine input (Joung et al., 2017) and lessened discharge (Fig. S.5) limiting mobilization from soils and litterfall. In contrast, many DOP compounds in May could have originated from the recent spring melt (Fig. S.5) flushing out autochthonous DOM that has accumulated underneath the ice (Rosenberg and Schroth, 2017) and loading anthropogenic DOP from the surface soils (Turner, 2005; Wagner et al., 2015; Brooker et al., 2018). This could partly explain why the DOP compositions in May were so different within the water column and between September and January in ESI (+) (Fig. 3).

4.3. Internal loading

Benthic DOM compositions in redox-dynamic freshwater are often controlled by the interplay of sorption/desorption processes with Fe minerals (Chassé and Ohno, 2016; Riedel et al., 2013; Dadi et al., 2017; Klein et al., 2019) and microbial processing (Kamjunke et al., 2017b; Mostovaya et al., 2017; Valle et al., 2018). These processes are a key component of the inorganic biogeochemical cycling within Missisquoi Bay (Smith et al., 2011; Schroth et al., 2015) and possibly DOM cycling. Across all samples, DO correlated positively with H/C and negatively with aromaticity, meaning saturated compounds were expected to increase in oxic waters, while aromatic and unsaturated DOM should be more abundant within oxygen-limiting conditions (Fig. 5). This is due to hypoxic conditions promoting reductive Fe(III) dissolution which releases larger, aromatic, and more oxygenated compounds into the overlying water by desorption (Riedel et al., 2013; Chassé and Ohno, 2016; Coward et al., 2018). Interestingly, NMDS biplots in both ionization modes indicated that the January bottom water was more similar to the September water column than the surface water from January, even though January in general had more saturated DOM (Fig. 2, Fig. 4). September retained a portion of allochthonous DOM in the water column (Fig. 6A), enriched in aromatic and oxygenated compounds that over time would adsorb onto mineral surfaces in the sediment (Riedel et al., 2013) as the bay froze over and riverine input was attenuated.

While aromatics were depleted in the January surface DOM, they were abundant in the bottom water during oxygen-limiting conditions, likely originating from reductive dissolution of poorly crystalline Fe(III) minerals that released these DOM compounds (Schroth et al., 2015; Joung et al., 2017).

Redox incubations from cores collected in May, September, and January (Fig. 7) afforded DOM that was more aliphatic, less aromatic, and smaller than the DOM prior to the incubations (Table 1), the opposite of what is expected to desorb from oxide mineral surfaces (Riedel et al., 2013). This compositional shift suggested that despite the presence of Mn(II) and some Fe(II) at the SWI (Fig. 7A,B,D), extensive desorption from Fe(III) mineral surfaces had not yet occurred at the surface in these incubations. Rather, this short-term anoxic period was characterized by a rapid shift to Mn(IV) reduction (Lovley, 1991) and was followed by the presence of aliphatic organic compounds likely from anaerobic microbial DOM processing (Boye et al., 2017; Valle et al., 2018; Valle et al., 2020). DOP compositions also responded in a similar way, producing more aliphatic and smaller compounds at the end of the incubations (Table S.3) suggesting that the sediment could be a source of bioavailable DOP compounds to the bottom water (Ahlgren et al., 2011; Parsons et al., 2017; Kurek et al., 2020). Furthermore, the DOP compositions released from the sediment followed a consistent pattern across all seasons (Table S.2; Table S.3), despite the seasonal variability in the sedimentary organic P biomolecular classes (Giles et al., 2015) and providing more evidence for benthic DOP being largely independent of riverine input and surface processes (Fig. 6B).

The results from the incubation experiments suggested that the benthic DOM released from initial short-term oxygen limitation events, such as bloom onset, was compositionally much different than DOM released from continual suboxic conditions such as during prolonged blooms or underneath ice cover (Table 1; Table S.3). By the end of the reduction period in all cores, microbial activity in the upper layers of the sediment was just beginning to reduce Fe(III) as Mn(IV) was being consumed (Fig. 7), and was accompanied by a flux of aliphatic and heteroatom-rich DOM and DOP compounds from porewaters (Table 1; Table S.3). Prolonged oxygen-limitation would have promoted greater reductive dissolution of Fe(III) oxyhydroxides, and eventually desorbed DOM into the bottom water that was more aromatic, such as in January (Fig. 4). While dissolution of these Fe(III) oxyhydroxides mobilizes much of the bioavailable orthophosphate into Missisquoi Bay (Smith et al., 2011; Giles et al., 2016), the initial pulse of DOM and DOP may also have a priming effect on the microbial communities, given that past studies have suggested DOM with similar aliphatic-like composition can be biolabile (D'Andrilli et al., 2015). Early release of autochthonous DOM during bloom formation might serve as a substrate for other microorganisms, particularly DOP that can be hydrolyzed to orthophosphate and consumed as a nutrient source during early bloom formation (Paerl and Otten, 2013). Excess P might further promote biomass growth, eventually leading to anoxic conditions in the bottom water, which could be responsible for most of the orthophosphate released from the sediments driving this feedback cycle (Smith et al., 2011; Giles et al., 2015; Giles et al., 2016).

4.4. DOM compositions across redox-dynamic freshwaters

DOM compositions have varied spatially within other redox-dynamic freshwaters (Gonsior et al., 2013; Dadi et al., 2017; Valle et al., 2020) and were driven by vertical mixing, adsorption, and biological processing. Some of these processes resulted from physiochemical conditions that influenced the overall seasonal DOM composition, such as pH and temperature, while others, like oxygen, influenced the spatial DOM distributions (Fig. 5). Geomorphology and hydrology have also driven much of the allochthonous composition within lakes (Kellerman et al., 2014; Kellerman et al., 2015). For instance, the large watershed-to-lake area ratio for Missisquoi Bay and its confined outlet topography provide a consistent source of terrestrial DOM and nutrients from various land types (e.g., agricultural, forested). Furthermore, these controls on basin-wide hydrodynamics impact the residence time of allochthonous DOM, and thus the opportunity for microbial processing during higher temperature periods, as seen across many high latitude lakes (Kellerman et al., 2014; Kellerman et al., 2015). Additionally, aquatic ecosystems can be influenced by DOP compositions (Baldwin, 2013) with high mineralization potential and utilization during each season (Bai et al., 2015), as suggested from this study and supported by previous work (Kurek et al., 2020). Therefore, we expect similar redox-dynamic lakes within a temperate climate to transform DOM both seasonally and spatially, while lakes that do not experience pronounced seasons and are relatively static in redox character would contain DOM that is more uniform, less diverse, and supplied from a regular source. We also expect other redox-driven eutrophic lakes to experience a similar DOP turnover between seasons and within water columns.

DOM compositions are complex and although SPE FT-ICR MS only provides a fraction of the compounds found in freshwaters, this same fraction was investigated consistently and revealed clear seasonal and spatial trends (Fig. 4). We also investigated a pool of DOM that was present in both ionization modes to make comparisons between depth, seasons, and sources more consistent. For instance, the riverine compounds common between both ionization modes (Fig. 6A, purple lines) followed the same trend while retaining a greater percentage of riverine DOM through the water column, suggesting that this portion of highly-ionizable DOM can also be a reliable of a tracer of allochthonous DOM in redox-dynamic freshwaters. By considering DOM in both modes, analytical sensitivity was increased, and the influence of low abundance ions unique to each ionization mode was minimized (Gonsior et al., 2011; Ohno et al., 2016; Hawkes et al., 2020). Additionally, The ESI (+) spectra were used to supplement the ESI (−) spectra, which are more commonly analyzed for DOM due to the broad range of carboxylic acids that are ionized (Sleighter and Hatcher, 2007). ESI (+) spectra also identified many additional N- and S-containing formulae, absent from ESI (−), that are thought to be characteristic of microbial DOM (Zhang et al., 2014) possibly accounting for the observed large unique fractions (Fig. 2; Fig. 6B).

DOP compositions also differed between ionization modes, sharing few formulae between the two (Fig. 3; Fig. 6B), and revealing a wide range of functional groups from various potential sources (Baldwin, 2013) that are not captured using ^{31}P NMR analysis. Although this study did not explicitly sample DOM and DOP during an active bloom, their compositions were detected in both ionization modes with clear differences before the bloom season (May), during an inter-bloom period (September), and at the end of the bloom season (January) (Fig. 4). Therefore, investigating the molecular characteristics using both ionization modes may be beneficial in identifying the role of DOM and DOP during ongoing early and late bloom events where the compositions are driven by both allochthonous and autochthonous sources containing various functional groups mobilized by redox gradients. By characterizing DOM and DOP compositions and identifying their physiochemical drivers we aim to gain insight into the scale of these transformations at the ecosystem level and further investigate the coupling of carbon and nutrient cycling with microbial communities within Missisquoi Bay as well as across other temperate aquatic systems.

5. Conclusion

Missisquoi Bay DOM composition varied both seasonally and spatially during a sampling year. Pre-bloom DOM was mainly composed of allochthonous CHO-containing formulae transported from the recent spring melt. Progression through the early summer bloom season transformed much of the aquatic DOM resulting in more N- and S-containing formulae with a strong uniformity within the water column as well as stable allochthonous input during baseflow conditions. The transition into colder temperatures in winter transformed less DOM than during the early bloom period, but was characterized by more aliphatic

compounds, likely from a shift to heterotrophy. Furthermore, the winter suboxic water retained many of the same summer terrestrial compounds, suggesting a pool of stable DOM was desorbed from the sediment during prolonged low oxygen conditions under ice cover, whereas reduced and aliphatic compounds were released from anaerobic porewaters at the onset of simulated hypoxic conditions. In contrast to DOM, DOP shared very few compounds within the water column, from different fluvial sources, and between other seasons, but was processed during the summer bloom period and coincided with quantitative changes in P speciation. These differences suggest aquatic DOP compositions are unique to each depth and season and may impact P bioavailability in redox-dynamic freshwaters.

Declaration of Competing Interest

The authors declare that there are no conflicts of interest.

Acknowledgements

Funding from the National Science Foundation SusChEM program (156093 to GKD and AWS) is gratefully acknowledged for support of this research. AWS also received funding from VT/NSF EPSCoR to support the collection of high-frequency monitoring data, and this material is based upon work supported by the National Science Foundation under VT EPSCoR (NSF OIA 1556770). We thank Dr. Robert Spencer for initial feedback on this work as well as Austin Wilkes, Megan Leduc, Wilton Burris, and Saul Blocher for their help with obtaining samples and QA/QC of the high frequency data.

Appendix A. Supplementary data

Supplementary data to this article can be found online at https://doi.org/10.1016/j.chemgeo.2021.120212.

References

Ahlgren, J., Reitzel, K., De Brabandere, H., Gogoll, A., Rydin, E., 2011. Release of organic P forms from lake sediments. Water Res. 45 (2), 565–572.
Bai, X.L., Zhou, Y.K., Sun, J.H., Ma, J.H., Zhao, H.Y., Liu, X.F., 2015. Classes of dissolved and particulate phosphorus compounds and their spatial distributions in the water of a eutrophic lake: a ^{31}P NMR study. Biogeochemistry 126 (1–2), 227–240.
Baldwin, D.S., 2013. Organic phosphorus in the aquatic environment. Environ. Chem. 10 (6), 439–454.
Baldwin, D., Howitt, J., Beattie, J., 2005. Abiotic degradation of organic phosphorus compounds in the environment. In: Organic Phosphorus in the Environment. CABI Publishing, Wallingford, UK, pp. 75–88.
Bittar, T.B., Stubbins, A., Vieira, A.A., Mopper, K., 2015a. Characterization and photodegradation of dissolved organic matter (DOM) from a tropical lake and its dominant primary producer, the cyanobacteria Microcystis aeruginosa. Mar. Chem. 177, 205–217.
Bittar, T.B., Vieira, A.A., Stubbins, A., Mopper, K., 2015b. Competition between photochemical and biological degradation of dissolved organic matter from the cyanobacteria Microcystis aeruginosa. Limnol. Oceanogr. 60 (4), 1172–1194.
Bowling, L.C., Blais, S., Sinotte, M., 2015. Heterogeneous spatial and temporal cyanobacterial distributions in Missisquoi Bay, Lake Champlain: an analysis of a 9 year data set. J. Great Lakes Res. 41 (1), 164–179.
Boye, K., Noël, V., Tfaily, M.M., Bone, S.E., Williams, K.H., Bargar, J.R., Fendorf, S., 2017. Thermodynamically controlled preservation of organic carbon in floodplains. Nat. Geosci. 10 (6), 415–419.
Brendel, P.J., Luther, G.W.I., 1995. Development of a gold amalgam voltammetric microelectrode for the determination of dissolved Fe, Mn, O2, and S (-II) in porewaters of marine and freshwater sediments. Environ. Sci. Technol. 29 (3), 751–761.
Brooker, M.R., Longnecker, K., Kujawinski, E.B., Evert, M., Mouser, P.J., 2018. Discrete Organic Phosphorus Signatures are Evident in Pollutant sources within a Lake Erie Tributary. Environ. Sci. Technol. 52 (12), 6771–6779.
Chassé, A.W., Ohno, T., 2016. Higher molecular mass organic matter molecules compete with orthophosphate for adsorption to iron (oxy) hydroxide. Environ. Sci. Technol. 50 (14), 7461–7469.
Cooper, W.T., Llewelyn, J.M., Bennett, G.L., Stenson, A.C., Salters, V.J., 2005. Organic phosphorus speciation in natural waters by mass spectrometry. In: Organic Phosphorus in the Environment. CABI Publishing, Wallingford, UK, pp. 45–74.
Core Team, R., 2020. R: A Language and Environment for Statistical Computing. R Foundation for Statistical Computing, Vienna, Austria. http://www.R-project.org/.
Coward, E.K., Ohno, T., Plante, A.F., 2018. Adsorption and molecular fractionation of dissolved organic matter on iron-bearing mineral matrices of varying crystallinity. Environ. Sci. Technol. 52 (3), 1036–1044.
Dadi, T., Harir, M., Hertkorn, N., Koschorreck, M., Schmitt-Kopplin, P., Herzsprung, P., 2017. Redox Conditions Affect Dissolved Organic Carbon Quality in Stratified Freshwaters. Environ. Sci. Technol. 51 (23), 13705–13713.
D'Andrilli, J., Foreman, C.M., Marshall, A.G., McKnight, D.M., 2013. Characterization of IHSS Pony Lake fulvic acid dissolved organic matter by electrospray ionization Fourier transform ion cyclotron resonance mass spectrometry and fluorescence spectroscopy. Org. Geochem. 65, 19–28.
D'Andrilli, J., Cooper, W.T., Foreman, C.M., Marshall, A.G., 2015. An ultrahigh-resolution mass spectrometry index to estimate natural organic matter lability. Rapid Commun. Mass Spectrom. 29 (24), 2385–2401.
Dittmar, T., Koch, B., Hertkorn, N., Kattner, G., 2008. A simple and efficient method for the solid-phase extraction of dissolved organic matter (SPE-DOM) from seawater. Limnol. Oceanogr. Methods 6 (6), 230–235.
Drake, T.W., Raymond, P.A., Spencer, R.G., 2018. Terrestrial carbon inputs to inland waters: a current synthesis of estimates and uncertainty. Limnol. Oceanogr. Lett. 3 (3), 132–142.
El-Rifai, H., Heerboth, M., Gedris, T.E., Newman, S., Orem, W., Cooper, W.T., 2008. NMR and mass spectrometry of phosphorus in wetlands. Eur. J. Soil Sci. 59 (3), 517–525.
Giles, C.D., Lee, L.G., Cade-Menun, B.J., Hill, J.E., Isles, P.D., Schroth, A.W., Druschel, G. K., 2015. Characterization of organic phosphorus form and bioavailability in lake sediments using ^{31}P nuclear magnetic resonance and enzymatic hydrolysis. J. Environ. Qual. 44 (3), 882–894.
Giles, C.D., Isles, P.D., Manley, T., Xu, Y., Druschel, G.K., Schroth, A.W., 2016. The mobility of phosphorus, iron, and manganese through the sediment–water continuum of a shallow eutrophic freshwater lake under stratified and mixed water-column conditions. Biogeochemistry 127 (1), 15–34.
Gonsior, M., Peake, B.M., Cooper, W.T., Podgorski, D.C., D'Andrilli, J., Dittmar, T., Cooper, W.J., 2011. Characterization of dissolved organic matter across the Subtropical Convergence off the South Island, New Zealand. Mar. Chem. 123 (1–4), 99–110.
Gonsior, M., Schmitt-Kopplin, P., Bastviken, D., 2013. Depth-dependent molecular composition and photo-reactivity of dissolved organic matter in a boreal lake under winter and summer conditions. Biogeosciences 10 (11), 6945–6956.
Gonsior, M., Valle, J., Schmitt-Kopplin, P., Hertkorn, N., Bastviken, D., Luek, J., Enrich Prast, A., 2016. Chemodiversity of dissolved organic matter in the Amazon Basin. Biogeosciences 13 (14), 4279–4290.
Guillemette, F., del Giorgio, P.A., 2012. Simultaneous consumption and production of fluorescent dissolved organic matter by lake bacterioplankton. Environ. Microbiol. 14 (6), 1432–1443.
Harrell Jr., F.E., 2020. Hmisc: Harrel Miscellaneous. R package version 4.4-0. https://cran.r-project.org/package=Hmisc.
Hawkes, J.A., D'Andrilli, J., Agar, J.N., Barrow, M.P., Berg, S.M., Catalán, N., Gavard, R., 2020. An international laboratory comparison of dissolved organic matter composition by high resolution mass spectrometry: are we getting the same answer? Limnol. Oceanogr. Methods 18 (6), 235–258.
Heath, R.T., 2005. Microbial turnover of organic phosphorus in aquatic systems. In: Organic Phosphorus in the Environment. CABI Publishing, Wallingford, UK, pp. 185–204.
Hertkorn, N., Ruecker, C., Meringer, M., Gugisch, R., Frommberger, M., Perdue, E.M., Schmitt-Kopplin, P., 2007. High-precision frequency measurements: indispensable tools at the core of the molecular-level analysis of complex systems. Anal. Bioanal. Chem. 389 (5), 1311–1327.
Hughey, C.A., Hendrickson, C.L., Rodgers, R.P., Marshall, A.G., Qian, K., 2001. Kendrick mass defect spectrum: a compact visual analysis for ultrahigh-resolution broadband mass spectra. Anal. Chem. 73 (19), 4676–4681.
Isles, P.D., Giles, C.D., Gearhart, T.A., Xu, Y., Druschel, G.K., Schroth, A.W., 2015. Dynamic internal drivers of a historically severe cyanobacteria bloom in Lake Champlain revealed through comprehensive monitoring. J. Great Lakes Res. 41 (3), 818–829.
Isles, P.D., Rizzo, D.M., Xu, Y., Schroth, A.W., 2017a. Modeling the drivers of interannual variability in cyanobacterial bloom severity using self-organizing maps and high-frequency data. Inland Waters 7 (3), 333–347.
Isles, P.D., Xu, Y., Stockwell, J.D., Schroth, A.W., 2017b. Climate-driven changes in energy and mass inputs systematically alter nutrient concentration and stoichiometry in deep and shallow regions of Lake Champlain. Biogeochemistry 133 (2), 201–217.
Johnston, S.E., Bogard, M.J., Rogers, J.A., Butman, D., Striegl, R.G., Dornblaser, M., Spencer, R.G., 2019. Constraining dissolved organic matter sources and temporal variability in a model sub-Arctic lake. Biogeochemistry 146 (3), 271–292.
Joung, D., Leduc, M., Ramcharitar, B., Xu, Y., Isles, P.D., Stockwell, J.D., Schroth, A.W., 2017. Winter weather and lake-watershed physical configuration drive phosphorus, iron, and manganese dynamics in water and sediment of ice-covered lakes. Limnol. Oceanogr. 62 (4), 1620–1635.
Kamjunke, N., Nimptsch, J., Harir, M., Herzsprung, P., Schmitt-Kopplin, P., Neu, T.R., Woelfl, S., 2017a. Land-based salmon aquacultures change the quality and bacterial degradation of riverine dissolved organic matter. Sci. Rep. 7, 43739.
Kamjunke, N., von Tümpling, W., Hertkorn, N., Harir, M., Schmitt-Kopplin, P., Norf, H., Herzsprung, P., 2017b. A new approach for evaluating transformations of dissolved organic matter (DOM) via high-resolution mass spectrometry and relating it to bacterial activity. Water Res. 123, 513–523.
Kellerman, A.M., Dittmar, T., Kothawala, D.N., Tranvik, L.J., 2014. Chemodiversity of dissolved organic matter in lakes driven by climate and hydrology. Nat. Commun. 5 (1), 1–8.

Kellerman, A.M., Kothawala, D.N., Dittmar, T., Tranvik, L.J., 2015. Persistence of dissolved organic matter in lakes related to its molecular characteristics. Nat. Geosci. 8 (6), 454.
Klein, A.R., Bone, S.E., Bakker, E., Chang, Z., Aristilde, L., 2019. Abiotic phosphorus recycling from adsorbed ribonucleotides on a ferrihydrite-type mineral: probing solution and surface species. J. Colloid Interface Sci. 547, 171–182.
Koch, B.P., Dittmar, T., 2006. From mass to structure: an aromaticity index for high-resolution mass data of natural organic matter. Rapid Commun. Mass Spectrom. 20 (5), 926–932.
Koch, B.P., Dittmar, T., 2016. From mass to structure: an aromaticity index for high-resolution mass data of natural organic matter. Rapid Commun. Mass Spectrom. 30, 250.
Koch, B.P., Witt, M., Engbrodt, R., Dittmar, T., Kattner, G., 2005. Molecular formulae of marine and terrigenous dissolved organic matter detected by electrospray ionization Fourier transform ion cyclotron resonance mass spectrometry. Geochim. Cosmochim. Acta 69 (13), 3299–3308.
Kurek, M.R., Harir, M., Shukle, J.T., Schroth, A.W., Schmitt-Kopplin, P., Druschel, G.K., 2020. Chemical fractionation of organic matter and organic phosphorus extractions from freshwater lake sediment. Anal. Chim. Acta 1130, 29–38.
Larsson, J., 2018. Eulerr: Area-Proportional Euler and Venn Diagrams with Ellipses. R Package Version 4.1.0. https://cran.r-project.org/package=eulerr.
Li, W., Joshi, S.R., Hou, G., Burdige, D.J., Sparks, D.L., Jaisi, D.P., 2014. Characterizing phosphorus speciation of Chesapeake Bay sediments using chemical extraction, 31P NMR, and X-ray absorption fine structure spectroscopy. Environ. Sci. Technol. 49 (1), 203–211.
Li, Y., Harir, M., Lucio, M., Kanawati, B., Smirnov, K., Flerus, R., Hertkorn, N., 2016. Proposed guidelines for solid phase extraction of Suwannee River dissolved organic matter. Anal. Chem. 88 (13), 6680–6688.
Llewelyn, J.M., Landing, W.M., Marshall, A.G., Cooper, W.T., 2002. Electrospray ionization Fourier transform ion cyclotron resonance mass spectrometry of dissolved organic phosphorus species in a treatment wetland after selective isolation and concentration. Anal. Chem. 74 (3), 600–606.
Lovley, D.R., 1991. Dissimilatory Fe (III) and Mn (IV) reduction. Microbiol. Rev. 55 (2), 259–287.
Ly, Q.V., Maqbool, T., Hur, J., 2017. Unique characteristics of algal dissolved organic matter and their association with membrane fouling behavior: a review. Environ. Sci. Pollut. Res. 24 (12), 11192–11205.
Mangal, V., Stock, N.L., Guéguen, C., 2016. Molecular characterization of phytoplankton dissolved organic matter (DOM) and sulfur components using high resolution Orbitrap mass spectrometry. Anal. Bioanal. Chem. 408 (7), 1891–1900.
Mann, B.F., Chen, H., Herndon, E.M., Chu, R.K., Tolic, N., Portier, E.F., Graham, D.E., 2015. Indexing permafrost soil organic matter degradation using high-resolution mass spectrometry. PLoS One 10 (6), e0130557.
Morling, K., Raeke, J., Kamjunke, N., Reemtsma, T., Tittel, J., 2017. Tracing aquatic priming effect during microbial decomposition of terrestrial dissolved organic carbon in chemostat experiments. Microb. Ecol. 74 (3), 534–549.
Mostovaya, A., Hawkes, J.A., Dittmar, T., Tranvik, L.J., 2017. Molecular determinants of dissolved organic matter reactivity in lake water. Front. Earth Sci. 5, 106.
Mur, R., Skulberg, O.M., Utkilen, H., 1999. Cyanobacteria in the environment. In: *Toxic Cyanobacteria* In *Water: A Guide To Their Public Health Consequences, Monitoring And Management*. CRC Press, pp. 15–40.
Nazari-Sharabian, M., Ahmad, S., Karakouzian, M., 2018. Climate change and eutrophication: a short review. Eng. Technol. Appl. Sci. Res. 8 (6), 3668–3672.
Ohno, T., Sleighter, R.L., Hatcher, P.G., 2016. Comparative study of organic matter chemical characterization using negative and positive mode electrospray ionization ultrahigh-resolution mass spectrometry. Anal. Bioanal. Chem. 408 (10), 2497–2504.
Oksanen, J., Blanchet, F.G., Kindt, R., Legendre, P., Minchin, P.R., O'hara, R.B., Oksanen, M.J., 2013. Package 'vegan'. Community Ecology Package, Version, 2(9).
O'neil, J.M., Davis, T.W., Burford, M.A., Gobler, C.J., 2012. The rise of harmful cyanobacteria blooms: the potential roles of eutrophication and climate change. Harmful Algae 14, 313–334.
Paerl, H.W., Otten, T.G., 2013. Harmful cyanobacterial blooms: causes, consequences, and controls. Microb. Ecol. 65 (4), 995–1010.
Paliy, O., Shankar, V., 2016. Application of multivariate statistical techniques in microbial ecology. Molecular ecology 25 (5), 1032–1057.
Parsons, C.T., Rezanezhad, F., O'Connell, D.W., Van Cappellen, P., 2017. Sediment phosphorus speciation and mobility under dynamic redox conditions. Biogeosciences 14 (14).
Perminova, I.V., Dubinenkov, I.V., Kononikhin, A.S., Konstantinov, A.I., Zherebker, A.Y., Andzhushev, M.A., Popov, I.A., 2014. Molecular mapping of sorbent selectivities with respect to isolation of Arctic dissolved organic matter as measured by Fourier transform mass spectrometry. Environ. Sci. Technol. 48 (13), 7461–7468.
Reynolds, C.S., Davies, P.S., 2001. Sources and bioavailability of phosphorus fractions in freshwaters: a British perspective. Biol. Rev. 76 (1), 27–64.
Riedel, T., Zak, D., Biester, H., Dittmar, T., 2013. Iron traps terrestrially derived dissolved organic matter at redox interfaces. Proc. Natl. Acad. Sci. 110 (25), 10101–10105.
Romano, S., Dittmar, T., Bondarev, V., Weber, R.J., Viant, M.R., Schulz-Vogt, H.N., 2014. Exo-metabolome of Pseudovibrio sp. FO-BEG1 analyzed by ultra-high resolution mass spectrometry and the effect of phosphate limitation. PLoS One 9 (5), e96038.
Rosenberg, B.D., Schroth, A.W., 2017. Coupling of reactive riverine phosphorus and iron species during hot transport moments: impacts of land cover and seasonality. Biogeochemistry 132 (1–2), 103–122.
Rozan, T.F., Taillefert, M., Trouwborst, R.E., Glazer, B.T., Ma, S., Herszage, J., Luther III, G.W., 2002. Iron-sulfur-phosphorus cycling in the sediments of a shallow coastal bay: Implications for sediment nutrient release and benthic macroalgal blooms. Limnol. Oceanogr. 47 (5), 1346–1354.
Schroth, A.W., Giles, C.D., Isles, P.D., Xu, Y., Perzan, Z., Druschel, G.K., 2015. Dynamic coupling of iron, manganese, and phosphorus behavior in water and sediment of shallow ice-covered eutrophic lakes. Environ. Sci. Technol. 49 (16), 9758–9767.
Shakeri Yekta, S., Gonsior, M., Schmitt-Kopplin, P., Svensson, B.H., 2012. Characterization of dissolved organic matter in full scale continuous stirred tank biogas reactors using ultrahigh resolution mass spectrometry: a qualitative overview. Environ. Sci. Technol. 46 (22), 12711–12719.
Sleighter, R.L., Hatcher, P.G., 2007. The application of electrospray ionization coupled to ultrahigh resolution mass spectrometry for the molecular characterization of natural organic matter. J. Mass Spectrom. 42 (5), 559–574.
Slowey, A.J., Marvin-DiPasquale, M., 2012. How to overcome inter-electrode variability and instability to quantify dissolved oxygen, Fe (II), Mn (II), and S (− II) in undisturbed soils and sediments using voltammetry. Geochem. Trans. 13 (1), 6.
Smith, V.H., Tilman, G.D., Nekola, J.C., 1999. Eutrophication: impacts of excess nutrient inputs on freshwater, marine, and terrestrial ecosystems. Environ. Pollut. 100 (1–3), 179–196.
Smith, L., Watzin, M.C., Druschel, G., 2011. Relating sediment phosphorus mobility to seasonal and diel redox fluctuations at the sediment–water interface in a eutrophic freshwater lake. Limnol. Oceanogr. 56 (6), 2251–2264.
Søndergaard, M., Jensen, J.P., Jeppesen, E., 2003. Role of sediment and internal loading of phosphorus in shallow lakes. Hydrobiologia 506 (1–3), 135–145.
Stubbins, A., Spencer, R.G., Chen, H., Hatcher, P.G., Mopper, K., Hernes, P.J., Six, J., 2010. Illuminated darkness: Molecular signatures of Congo River dissolved organic matter and its photochemical alteration as revealed by ultrahigh precision mass spectrometry. Limnol. Oceanogr. 55 (4), 1467–1477.
Swensen, M.M., Oyler, A.R., Minor, E.C., 2014. Rapid solid phase extraction of dissolved organic matter. Limnol. Oceanogr. Methods 12, 713–728.
Tranvik, L.J., Downing, J.A., Cotner, J.B., Loiselle, S.A., Striegl, R.G., Ballatore, T.J., Kortelainen, P.L., 2009. Lakes and reservoirs as regulators of carbon cycling and climate. Limnol. Oceanogr. *54* (6 part 2), 2298–2314.
Turner, B.L., 2005. Organic phosphorus transfer from terrestrial to aquatic environments. In: Organic Phosphorus in the Environment. CABI Publishing, Wallingford, UK, pp. 269–294.
Valle, J., Gonsior, M., Harir, M., Enrich-Prast, A., Schmitt-Kopplin, P., Bastviken, D., Conrad, R., Hertkorn, N., 2018. Extensive processing of sediment pore water dissolved organic matter during anoxic incubation as observed by high-field mass spectrometry (FTICR-MS). Water Res. 129, 252–263.
Valle, J., Harir, M., Gonsior, M., Enrich-Prast, A., Schmitt-Kopplin, P., Bastviken, D., Hertkorn, N., 2020. Molecular differences between water column and sediment pore water SPE-DOM in ten Swedish boreal lakes. Water Res. 170, 115320.
Voegelin, A., Senn, A.C., Kaegi, R., Hug, S.J., Mangold, S., 2013. Dynamic Fe-precipitate formation induced by Fe (II) oxidation in aerated phosphate-containing water. Geochim. Cosmochim. Acta 117, 216–231.
Wagner, S., Riedel, T., Niggemann, J., Vähätalo, A.V., Dittmar, T., Jaffé, R., 2015. Linking the molecular signature of heteroatomic dissolved organic matter to watershed characteristics in world rivers. Environ. Sci. Technol. 49 (23), 13798–13806.
Wang, X., Liu, F., Tan, W., Li, W., Feng, X., Sparks, D.L., 2013. Characteristics of phosphate adsorption-desorption onto ferrihydrite: comparison with well-crystalline Fe (hydr) oxides. Soil Sci. 178 (1), 1–11.
Wickham, H., 2016. ggplot2: Elegant Graphics for Data Analysis. Springer.
Zhang, F., Harir, M., Moritz, F., Zhang, J., Witting, M., Wu, Y., Hertkorn, N., 2014. Molecular and structural characterization of dissolved organic matter during and post cyanobacterial bloom in Taihu by combination of NMR spectroscopy and FTICR mass spectrometry. Water Res. 57, 280–294.